

Computational prediction of new magnetic materials

Cite as: J. Chem. Phys. **157**, 124704 (2022); <https://doi.org/10.1063/5.0113745>

Submitted: 24 July 2022 • Accepted: 15 August 2022 • Published Online: 29 September 2022

 Saeed Rahmanian Koshkaki,  Zahed Allahyari,  Artem R. Oganov, et al.



View Online



Export Citation



CrossMark

ARTICLES YOU MAY BE INTERESTED IN

[Computing chemical potentials of solutions from structure factors](#)

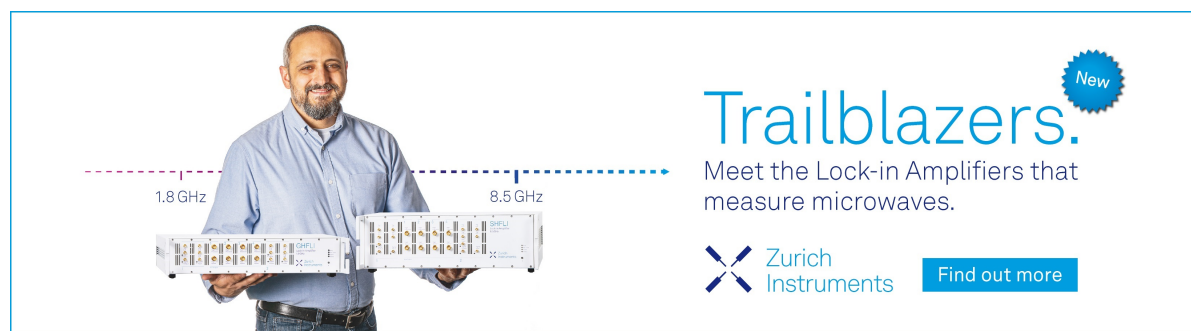
The Journal of Chemical Physics **157**, 121101 (2022); <https://doi.org/10.1063/5.0107059>


[Chemical design by artificial intelligence](#)

The Journal of Chemical Physics **157**, 120401 (2022); <https://doi.org/10.1063/5.0123281>


[On the nature of the chemical bond in valence bond theory](#)

The Journal of Chemical Physics **157**, 090901 (2022); <https://doi.org/10.1063/5.0095953>



Trailblazers. 

Meet the Lock-in Amplifiers that measure microwaves.

 Zurich Instruments [Find out more](#)

Computational prediction of new magnetic materials

Cite as: J. Chem. Phys. 157, 124704 (2022); doi: 10.1063/5.0113745

Submitted: 24 July 2022 • Accepted: 15 August 2022 •

Published Online: 29 September 2022



View Online



Export Citation



CrossMark

Saeed Rahmanian Koshkaki,^{1,2,3,a)} Zahed Allahyari,^{1,b)} Artem R. Oganov,^{1,b)}
Vladimir L. Solozhenko,⁴ Ilya B. Polovov,⁵ Alexander S. Belozеров,^{1,6} Andrey A. Katanin,^{1,2,6}
Vladimir I. Anisimov,^{1,5,6} Evgeny V. Tikhonov,^{1,7} Guang-Rui Qian,⁷ Konstantin V. Maksimtsev,⁵
Andrey S. Mukhamadeev,⁵ Andrey V. Chukin,⁵ Aleksandr V. Korolev,^{5,6} Nikolay V. Mushnikov,^{5,6}
and Hao Li^{1,8,9}

AFFILIATIONS

¹Skolkovo Institute of Science and Technology, 30 Bldg. 1, Bolshoy Blvd., Moscow 121205, Russia

²Moscow Institute of Physics and Technology, 9 Institutskiy Lane, Dolgoprudny 141700, Russia

³Department of Physics, The University of Texas at Dallas, Richardson, Texas 75080, USA

⁴LSPM-CNRS, Universite Sorbonne Paris Nord, 93430 Villetaneuse, France

⁵Ural Federal University, Mira Str. 19, 620002 Ekaterinburg, Russia

⁶M.N. Mikheev Institute of Metal Physics UB RAS, S. Kovalevskaya Str., 18, 620108 Ekaterinburg, Russia

⁷International Center for Materials Discovery, Northwestern Polytechnical University, Xi'an 710072, China

⁸CAS Key Laboratory of Functional Materials and Devices for Special Environments, Xinjiang Technical Institute of Physics & Chemistry, CAS, and Xinjiang Key Laboratory of Electronic Information Materials and Devices, 40-1 South Beijing Road, Urumqi 830011, China

⁹Center of Materials Science and Optoelectronics Engineering, University of Chinese Academy of Sciences, Beijing 100049, China

^{a)} Author to whom correspondence should be addressed: rahmanian@utdallas.edu

^{b)} E-mail: Z.Allahyari@skoltech.ru and A.Oganov@skoltech.ru

ABSTRACT

The discovery of new magnetic materials is a big challenge in the field of modern materials science. We report the development of a new extension of the evolutionary algorithm USPEX, enabling the search for half-metals (materials that are metallic only in one spin channel) and hard magnetic materials. First, we enabled the simultaneous optimization of stoichiometries, crystal structures, and magnetic structures of stable phases. Second, we developed a new fitness function for half-metallic materials that can be used for predicting half-metals through an evolutionary algorithm. We used this extended technique to predict new, potentially hard magnets and rediscover known half-metals. In total, we report five promising hard magnets with high energy product ($|BH|_{MAX}$), anisotropy field (H_a), and magnetic hardness (κ) and a few half-metal phases in the Cr–O system. A comparison of our predictions with experimental results, including the synthesis of a newly predicted antiferromagnetic material ($WMnB_2$), shows the robustness of our technique.

Published under an exclusive license by AIP Publishing. <https://doi.org/10.1063/5.0113745>

I. INTRODUCTION

Modern technology would be impossible without magnetic materials. Enhancing the useful properties of magnetic materials while making them lighter and cheaper would facilitate the application of these materials in modern and future technologies. Two types of technologically appealing magnetic materials are considered here: hard magnets and half-metals. The discovery of hard magnets

goes back half a century, when permanent rare earth-based magnets were discovered.¹ Many technologies and devices were developed using these hard magnets, but in the past three decades, there has been no significant achievement in the discovery of new hard magnets. At the same time, a new field of electronic technology known as spin-electronics (spintronics) is emerging, with promise in regard to the utilization of electron's spin degree of freedom to carry out logic operations and storage.^{2,3} 100% of the spin-polarized current

is needed, so having new materials for producing a fully polarized current at room temperature is a prerequisite.

One may divide ferromagnetic (FM) materials into two categories: *soft magnets* such as annealed iron, which can be magnetized easily but also easily demagnetized, and *hard magnets*, which tend to stay magnetized. Permanent magnets are based on hard magnets such as alnico, ferrite, or alloys of rare earth metals (i.e., Nd-Fe-B and Sm-Co types). There are four most important properties of a hard magnet: remanence (spontaneous magnetization M_0), Curie temperature T_c , coercivity (H_c), and energy product $|BH|_{\text{MAX}}$. These properties are determined by the local magnetic moment, exchange interaction, and spin-orbit coupling. Hard magnets should include (1) heavy atoms to create strong spin-orbit coupling, a relativistic effect solely responsible for fixing the direction of magnetization—among non-radioactive elements, spin-orbit coupling is strongest in Bi, Pb, Re, W, Ta, Hf, rare earths, Sb, Sn, Cd, Ag, Mo, and Zn; (2) transition metals—such as Fe, Co, Mn, or Ni—which are good donors of spin density because of the nearly half-filled d orbitals; and (3) some additional elements to broaden the chemical space and increase the likelihood of finding stable hard magnets.

The scarcity of rare earth elements creates the need for high-performance magnetic materials without rare earth elements.⁴ Computational search for promising magnetic materials is very useful since experimental studies are hindered by high cost and time-consuming procedure of synthesis; it is in fact impossible to exhaustively search for promising materials only by experiment. By means of recent developments in computational/theoretical materials science,^{5,6} several computational methods have been proposed for automated screening based on density functional theory (DFT) coupled with either data mining procedures⁷ or global optimization using, for example, evolutionary algorithms.^{8–12} In this study, we extend our evolutionary algorithm USPEX^{8,9,13,14} and run magnetic structure prediction at spin-polarized generalized gradient approximation (GGA)¹⁵ and GGA + U ^{16,17} levels of theory. We performed variable-composition searches for stable ferromagnetic compounds containing a heavy atom to provide strong spin-orbit coupling, a transition metal to increase the number of unpaired electrons, and optionally an additional element to stabilize the compound. These calculations produced a set of stable compounds, with detailed chemical formulas, and optimal arrangement of atoms and their magnetic moments.

II. COMPUTATIONAL METHODS

The evolutionary algorithm (USPEX) used here is capable of predicting stable structures/compositions formed by given elements. Details of the method are provided in Refs. 8, 9, and 13, and a number of applications (e.g., [18–24]) illustrate its efficacy in the case of atomic and molecular crystals, surfaces, two-dimensional materials, polymers, and nanoparticles. Here we use the variable-composition mode of USPEX,¹³ sampling structures with up to 16 atoms in the primitive cell. 60% of the highest-ranked structures were allowed to produce offspring using different variation operators—heredity and mutation. In each generation (except the first generation), 40% of structures were generated using heredity, 40% were generated by mutation (15% by softmutation, 15% by transmutation, and 10%

using spin mutation), and 20% were generated randomly. For binary systems (i.e., Cr-O, Fe-Sn, and Mn-Sn), the initial population size (number of randomly generated structures in the first generation) is equal to 160 and the normal population size (number of structures of next generations) is equal to 80. For ternary systems (i.e., W-Mn-B), these numbers are increased to 200 and 120, respectively.

The underlying structure relaxations and energy calculations were performed using the *Vienna Ab initio Simulation Package* (VASP) code^{25–28} at zero pressure. To reveal the ground state of magnetic materials, one needs to predict the optimal arrangement of local magnetic moments simultaneously with global optimization of the crystal structure, but an exhaustive sampling of all possible magnetic configurations for all produced crystal structures is often impractical. Here, we simplified the problem by considering only collinear magnetic systems—ferromagnetic (FM), antiferromagnetic (AFM), ferrimagnetic (FiM), and nonmagnetic (NM). Atoms in magnetically ordered phases can be in different spin states: high-spin (HS), low-spin (LS), various intermediate-spin (IS) states; moreover, in the same material, different spin states can coexist (LH, LI, IH). To that end, a new operator, spin mutation, was added to vary the magnitude and direction of magnetic moments on randomly selected atoms (for details of this new operator, we refer to the [supplementary material](#)).

Many magnetic materials are strongly correlated and one often has to go beyond DFT or DFT + U approaches. For several known materials, we carefully took electronic correlations into account using the DFT + U method^{29–32} and the dynamical mean-field theory (DMFT).^{33,34} The latter approach provides a systematic treatment of many-body effects by considering the local spin dynamics. A combination of DFT and DMFT, known as the DFT + DMFT approach,³⁵ has become a state-of-the-art method for providing a realistic description of correlated materials (for a review, see [36] and [37]). Our DMFT calculations were performed in the paramagnetic (spin symmetric) phase using the AMULET code.³⁸ The impurity problem was solved by the hybridization-expansion continuous-time quantum Monte Carlo algorithm with the density-density form of Coulomb interaction. The double-counting correction was taken in the around mean-field form. The Coulomb interaction matrix for d -shells was parameterized via Slater integrals F^0, F^2, F^4 linked to the Hubbard $U = F^0$ and Hund's rule coupling $J = (F^2 + F^4)/14$ (details can be found in 39).

In order to study half-metals, accurate band gaps are needed, and for this reason, the HSE06^{40,41} hybrid functional was used to calculate band structures and density of states (DOS) for the phases in the Cr-O system that were identified as the most promising in an USPEX search (see Fig. S4 in the [supplementary material](#)); these calculations were done using the PWmat^{42,43} code. The spin-polarized calculations were performed using NCPP-SG15-PBE pseudopotential with an energy cutoff of 680 eV and appropriate Monkhorst-Pack k -mesh with a resolution of $2\pi \times 0.06 \text{ \AA}^{-1}$.

A. Hard magnets

For all the selected systems, after finding the best structures using USPEX with $U - J = 0$ eV, the top 60–80 ranked structures were chosen for further investigation of their hard magnetic properties. To explore electron correlation effects, all selected structures were relaxed again at different values of $(U - J)$. To explore potential hard magnets, for each promising material we calculated

the magnetocrystalline anisotropy energy (MAE) curve. The MAE curve was calculated using a computationally efficient method implemented in VASP. In this method, initially, we performed a high-precision magnetic calculation (collinear calculation) to obtain the magnetic ground state, charge density, and wavefunction, then we added spin-orbit coupling and used the charge density and wavefunction obtained in the first step for calculating the ground state energy for different magnetization directions (noncollinear calculation). In this method, to optimize the calculation time, the initial calculation (collinear) is performed self-consistently, and then for the rotation of the magnetization direction (noncollinear), the non-self-consistent method implemented in VASP was used.⁴⁴ (For more details on the convergence of the MAE curve calculation, please refer to the [supplementary material](#).)

For DFT + U calculations, we used Dudarev's formula,¹⁷ which needs only one parameter, i.e., ($U - J$), for running the DFT + U calculation. In finding the MAE curve, we used the plane wave kinetic energy cutoff of 600 eV, and for each material and different values of $U - J$, we carefully checked the energy convergence with changing k-point mesh density to achieve the required excellent convergence of the energies and structural parameters. All the studied compounds are metallic and one expects that on-site electron correlations of 3d-electrons are to a large extent (but not completely) screened. We explored these phases at $0 \leq U - J \leq 2$ eV to account for the uncertainty of the extent of electron correlation in each compound. We then calculated the MAE curve, maximum energy product $|BH|_{\text{MAX}}$, magnetic hardness, and the anisotropy field (H_a) for selected structures. In the calculation of the MAE curve and anisotropy constants, we used an automatic k-point generator implemented in VASP and rotated the magnetization angle to find directions with the lowest and highest energy. The difference between these two energies gives the MAE and the corresponding curve is called the MAE curve. To calculate the MAE curve and, subsequently, hard magnetic properties, we used the uniaxial anisotropy expression; this approximation provides a simple but powerful parameterization of the magnetic anisotropy.⁴⁵ In this approximation, the MAE curve can be quantified by fitting energies to the following expression:

$$\frac{E}{V} = K_1 \sin^2 \alpha + K_2 \sin^4 \alpha, \quad (1)$$

where K_1 and K_2 are the first and second anisotropy constants, respectively, α is the angular change along the MAE curve, and V is the volume of the unit cell. Using this approximation, two different types of anisotropy are possible: easy axial and easy planar anisotropy. In easy axial anisotropy, $K_1 < 0$, and for easy planar anisotropy, $K_1 > 0$; here, we report the absolute value of K_1 and K_2 and mention whether it corresponds to easy axial/planar in a separate column of [Table II](#).

For each magnetic structure, we can define the magnetization vector in the Cartesian coordinate system as

$$M = M_0(\sin \theta \cos \phi \hat{x} + \sin \theta \sin \phi \hat{y} + \cos \theta \hat{z}), \quad (2)$$

where M_0 represents spontaneous magnetization, $(\hat{x}, \hat{y}, \hat{z})$ are the coordinates of the unit vector of magnetization, and θ and ϕ are the angles of Cartesian coordinates retrieved from spherical

coordinates (radius M_0 , inclination θ , azimuth ϕ). Using the single-domain crystal assumption with coherent rotation of magnetization for ferromagnetic phases, we compute the anisotropy field in the ferromagnetic Stoner-Wohlfarth (SW) model as follows:

$$H_a = 2 \frac{K_1}{\mu_0 M_0} \quad (\text{for } K_1 > 0). \quad (3)$$

Here, we ignored K_2 since all predicted materials in this work have $K_2 \approx 0$. By calculating the magnetization M_0 , one can calculate the energy product ($|BH|_{\text{MAX}}$), which is the absolute upper limit of magnetostatic energy stored in free space by a permanent magnet of unit volume.⁴⁵ $|BH|_{\text{MAX}}$ for an ideal square hysteresis loop⁴ is given by

$$|BH|_{\text{MAX}} = \frac{\mu_0 M_0^2}{4}, \quad (4)$$

where μ_0 is the vacuum permeability ($\mu_0 = 4\pi \times 10^{-7}$ NA⁻²).

Another important quantity in characterizing hard magnets concerns the possibility to fabricate a magnet in any shape without losing its magnetization;⁴ this dimensionless quantity is known as magnetic hardness (κ),

$$\kappa = \sqrt{\frac{K_1}{\mu_0 M_0^2}}, \quad (5)$$

for an optimized single-domain permanent magnet to have $H_c > M_0/2$, a value of $\kappa > 1$ is expected (this condition may change depending on the desired macroscopic shape of the magnet, e.g., long needle or thin film).

B. Half-metals

High signal strength and robust readout in spin-electronic devices can be achieved with the use of fully polarized current.^{46,47} One way to achieve 100% polarization is to use half-metals as spin filter. Half-metals have the intrinsic ability to produce spin-polarized electronic current. In a half-metal, the density of states (DOS) at the Fermi level $g(E_f)$ for one spin direction is zero (usually minority band) and that for the other spin direction is nonzero $g(E_f)$ (one spin channel is insulating, while the other is conducting).⁴⁸ In 1983, de Groot *et al.* reported half-metallic Heusler alloys as other experimental and theoretical reports of new half-metals appeared, including two famous half-metals: rutile-structured CrO₂ and Heusler alloy NiMnSb.⁴⁸ While many works have tried to predict new half-metal candidates,⁵⁰⁻⁵⁴ to date, a reliable, fast, low-cost, and general method of discovery is lacking. One of the main disadvantages of current half-metals is their strong temperature dependence of current polarization, which has roots in spin wave excitation and a narrow gap between the Fermi energy and top of the conduction band in the insulating channel.⁴⁷

Using the density of states (DOS) at the Fermi energy, we define the spin polarization to be⁵⁵

$$P(E_f) = \left| \frac{g_{\uparrow}(E_f) - g_{\downarrow}(E_f)}{g_{\uparrow}(E_f) + g_{\downarrow}(E_f)} \right|, \quad (6)$$

where $g_{\uparrow}(E_f)$ and $g_{\downarrow}(E_f)$ are the densities of states at the Fermi level for the spin channels. One major reason for this temperature dependence is the location of the Fermi energy near the top (bottom) of valence (conduction) band in the insulating channel. In this section,

we introduce a new fitness function to find materials that do not suffer from this problem. To achieve 100% spin polarization, one spin channel should be insulating (semiconducting) and the other one conducting. Moreover, to achieve good conductivity, the conducting spin channel should have high enough DOS at the Fermi level ($(g(E_f))_{\text{cond}}$). The fitness function that embodies all this information in the form of a single number is (with unit of \AA^{-3})

$$f_{HM} = \left(\frac{E_C \times E_V}{E_g} \right)_{\text{ins}} \times (g(E_f))_{\text{cond}}, \quad (7)$$

where E_C and E_V are the energy difference between the Fermi energy and bottom of conduction band and that between the Fermi energy and top of the valance band, respectively, E_g is the energy bandgap ($E_g = E_C + E_V$), and $(g(E_f))_{\text{cond}}$ is the density of states (in states/eV \AA^3) for the conducting spin channel (all E_g , E_C , and E_V are defined for the insulating channel). The advantage of this new fitness function is that it can measure the bandgap and DOS simultaneously.

Multi-objective (MO) optimization^{56,57} mode of USPEX was used to ensure that structures obtained through the evolutionary search are both good half-metals and energetically favorable. It is important to use this method since unstable half-metals are as

useless as stable compounds with no half-metallicity, and both properties need to be optimized simultaneously—see Fig. 1.

III. RESULTS

A. Half-metals

To test our fitness function and its working within USPEX, we chose the well-studied Cr–O system. In this system, we expect to find the known half-metal CrO_2 . In this calculation, we employed the multi-objective optimization method^{56,57} in order to search for phases with low energy and high half-metallicity simultaneously. We performed a USPEX search in the Cr–O system using the DFT+U method based on GGA-PBE functional¹⁵ with $U - J = 2.1$ and 3.7 eV (typical values used by previous studies on this system^{58–60}). These calculations were carried out using the variable-composition mode¹³ of USPEX, to screen all the possible compounds in this system. As a result, several promising phases were predicted. Among these, all the reported stable phases⁶¹ were indeed found. Our calculations show that $R3c - \text{Cr}_2\text{O}_3$ is stable at $U - J = 2.1$ and 3.7 eV, which is in agreement with previous studies.^{58,59} $P4_2/mnm - \text{CrO}_2$ is stable at $U - J = 2.1$ eV and metastable (45 meV/atom above convex hull) at $U - J = 3.7$ eV. Several geometrically similar structures of CrO with space groups

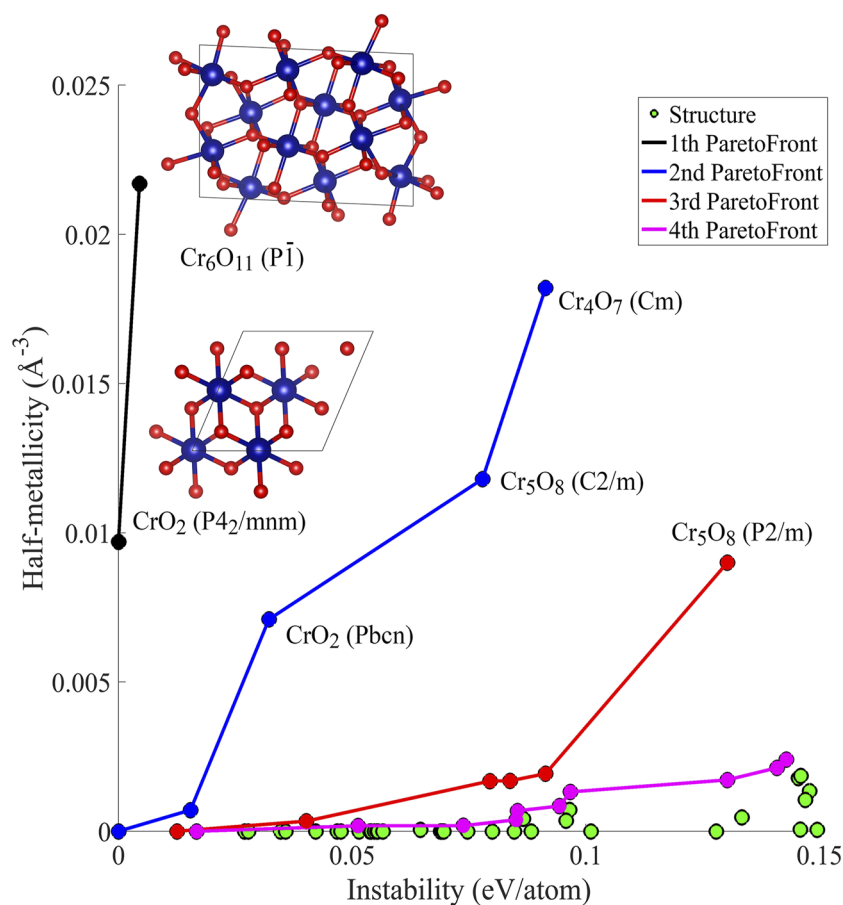


FIG. 1. Ashby plot of half-metallicity vs instability of Cr–O compounds. The values were obtained using HSE06 hybrid functional. Structures on the first Pareto front are embedded in the plot.

Cccm, *C2/c*, and *P4₂/mmc* were predicted. Our calculation shows that the energy of *Cccm*-CrO is slightly lower, and this structure is thermodynamically stable at $U - J = 3.7$ eV and metastable at $U - J = 2.1$ eV (12 meV/atom above convex hull). The phase diagram of this system is shown in Fig. 2(a). We find that Cr_5O_{12} is metastable with energy 17 and 133 meV/atom above the convex hull for $U - J = 2.1$ and 3.7 eV, respectively (in agreement with other works⁶²). In addition to the prediction of all reported low-energy chromium oxides, we predicted several new promising phases with low energy and/or high half-metallicity. Metastable low-energy phases $P1\text{-Cr}_3\text{O}_4$ (with energy 15 meV/atom above the convex hull) and $C2/m\text{-Cr}_5\text{O}_8$, $P2/m\text{-Cr}_5\text{O}_8$, and $Cm\text{-Cr}_4\text{O}_7$ with high half-metallicity were predicted by our calculations and are shown in Table I.

Looking at Table I, one can see that several phases are predicted with high half-metallicity. The predicted $P4_2/mmm\text{-CrO}_2$ was found to be a half-metal, and its crystal structure is in excellent agreement with experiment^{63,64} (see Table I). Along with this phase, two very promising half-metal phases are Cr_6O_{11} and Cr_4O_7 with

energies very close to the convex hull. All these phases are also predicted to have high magnetization. In recent years, many attempts to find of new half-metals—from 2D systems^{52,53} to Heusler alloys⁵¹—have been made. In this work, we defined a simple and physically reasonable fitness function for half-metals and showed that the extension of evolutionary algorithm USPEX by the introduced fitness function is a powerful tool for a systematic search for this class of materials and can facilitate the discovery of new half-metals.

B. Hard magnets

Finding rare earth-free hard magnets. One has to keep in mind that finding rare earth-free hard magnets is a challenging task; here, we picked stable and metastable phases, which have at least one of the selected hard magnet properties: spontaneous magnetization (M_0), anisotropy field (H_a), magnetic hardness (κ), energy product ($|BH|_{\text{MAX}}$). As a benchmark, we also calculated the hard magnetic properties of FePt, a well-known hard magnet, and our results are in very good agreement with the actual properties of FePt, see Table II.

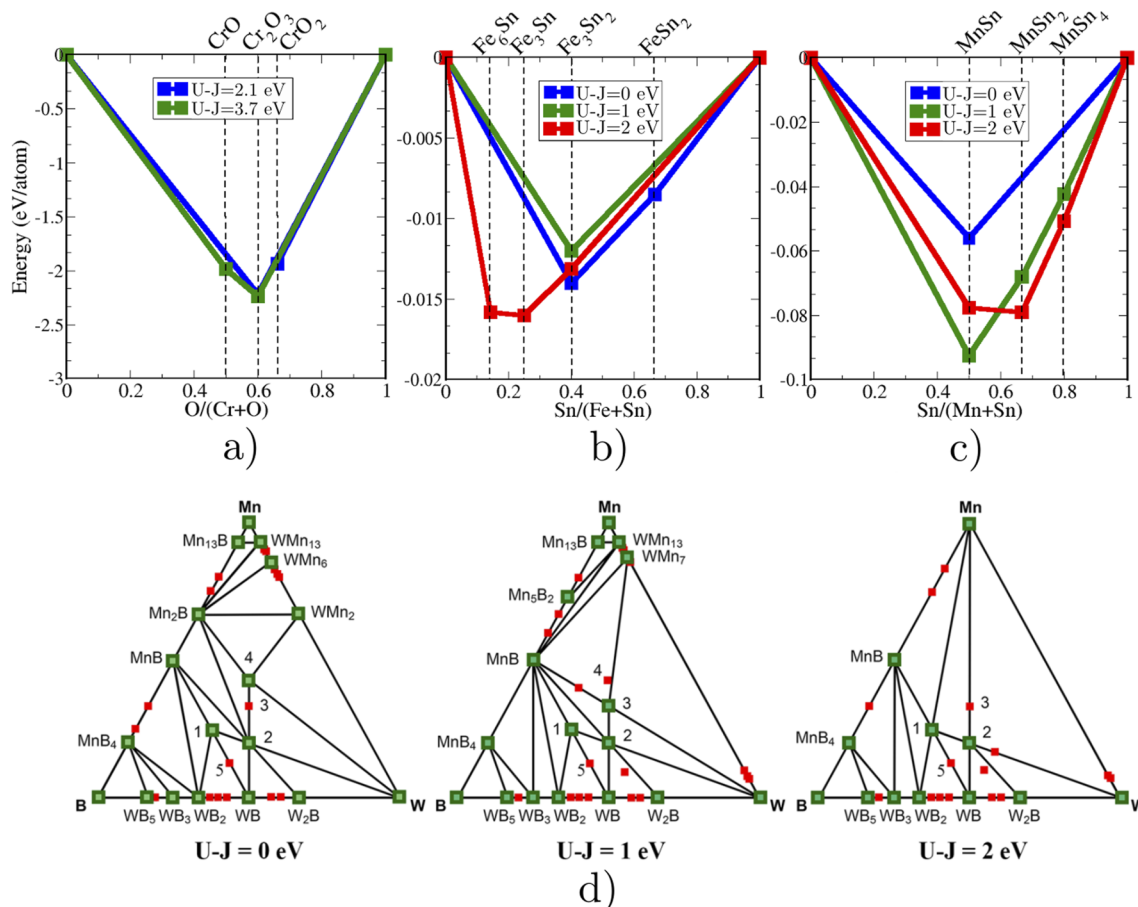


FIG. 2. Convex hulls of (a) Cr–O, (b) Fe–Sn, (c) Mn–Sn, and (d) W–Mn–B systems. In the ternary case, green points indicate stable phases and red points show metastable phases. It is worth mentioning that the stability of one structure with one value of $U - J$ does not guarantee stability for other values of $U - J$; for more details on the range of stability of selected compound with the change of $U - J$, see the [supplementary material](#).

TABLE I. Structural parameters and half-metallicity (f_{HM}) of the predicted chromium oxides. Structures were relaxed using DFT+U (at $U - J = 2.1$ eV), while the electronic properties (including the half-metallicity) were calculated using HSE06 hybrid functional.

Compounds	Space Group	Magnetization	$f_{HM} \times 10^3$	Lattice parameters						ΔH (eV/atom)	E above convex hull (eV/atom)
		$\mu_B \cdot \text{\AA}^{-3}$	\AA^{-3}	a (Å)	b (Å)	c (Å)	α	β	γ		
CrO ₂	P4 ₂ /mnm	0.068	9.7	4.49	4.49	2.98	90.0	90.0	90.0	-1.935	0
Cr ₂ O ₃	R3c	0.115	0.0	5.09	5.09	13.76	90.0	90.0	120.0	-2.216	0
Cr ₆ O ₁₁	PI	0.081	21.7	9.58	7.06	5.45	72.3	81.1	89.7	-2.013	0.004
CrO	Cccm	0.147	0.0	4.02	4.69	5.46	90.0	90.0	90.0	-1.834	0.012
Cr ₃ O ₄	PI	0.120	0.7	5.43	3.05	5.16	88.3	73.3	96.0	-2.095	0.015
CrO ₂	Pbcn	0.069	7.1	4.31	5.51	5.02	90.0	90.0	90.0	-1.903	0.032
Cr ₂ O ₃	R3	0.108	0.0	5.15	5.15	14.37	90.0	90.0	120.0	-2.162	0.055
Cr ₅ O ₈	C2/m	0.095	11.8	10.10	2.96	10.16	90.0	105.2	90.0	-2.073	0.078
Cr ₄ O ₇	Cm	0.069	18.2	12.32	3.03	10.08	90.0	129.5	90.0	-1.971	0.091
Cr ₅ O ₈	P2/m	0.091	9.0	5.21	3.00	9.90	90.0	100.3	90.0	-2.021	0.130
Experimental											
CrO ₂ ⁶⁵	P4 ₂ /mnm			4.42	4.42	2.92	90.0	90.0	90.0	-2.066 ⁶⁶	0
Cr ₂ O ₃ ⁶⁷	R3c			5.07	5.70	13.87	90.0	90.0	120	-2.367 ⁵⁹	0

C. W-Mn-B system

In W-Mn-B systems, tungsten plays the role of a heavy element and manganese is a donor of spin density. Boron was added to broaden the chemical space and stabilize additional compounds. We used the evolutionary algorithm USPEX with $U - J = 0$ eV to search

for stable compounds in the W-Mn-B system in 80 generations (exploring about 9600 structures with different stoichiometries). All the energy calculations and structure relaxations in USPEX were done using spin-polarized GGA-PBE functional and VASP code.

TABLE II. Properties of our predicted compounds, compared with modern permanent magnets obtained experimentally (FePt, Sm₂Co₁₇, Nd₂Fe₁₄B, and Sm₂Fe₁₇N₃).⁸⁴

Compound	Space group	($U - J$) (eV)	M_0 (MA/m)	$ K_1 $ (MJ/m ³)	$ K_2 $ (MJ/m ³)	MAE (MJ/m ³)	κ	H_a (T)	$ BH _{MAX}$ (KJ m ⁻³)	Easy axis/plane
W ₃ MnB ₄	<i>Pmm2</i>	0	0.25	2.76	...	2.76	5.92	22.0	19.7	...
	<i>Pmm2</i>	1	0.28	4.3	...	4.30	6.52	30.3	25.2	...
	<i>Pmm2</i>	2	0.32	5.70	...	5.70	6.63	35.5	32.4	...
FeSn ₂	<i>I4/mcm</i>	0	0.257	1.89	0.0	1.89	4.76	16.7	20.7	Easy plane
Fe ₃ Sn	<i>P6₃/mmc</i>	0	1.15	1.08	0.0	1.08	0.80	1.87	416	Easy plane
	<i>P6₃/mmc</i>	2	1.32	0.16	0	0.16	0.27	0.23	545	Easy axis
	<i>P6/mmm</i>	0	0.58	0.73	0.2	0.86	1.44	3.00	105	Easy axis
MnSn	<i>P6/mmm</i>	1	0.72	0.67	0.10	0.65	1.00	1.81	164	Easy plane
	<i>P6/mmm</i>	2	0.78	0.79	0.01	0.86	1.06	2.2	192	Easy plane
MnSn ₄	<i>Cmmm</i>	1	0.23	1.20	0.01	1.19	4.18	10.2	17.1	Easy axis
	<i>Cmmm</i>	2	0.25	0.91	0.04	0.96	3.47	7.60	19.9	Easy axis
FePt		0	1.09	13.8	0.31	14.1	3.06	25.8	375	Easy axis
		1	1.14	11.5	0.20	11.7	2.7	20.6	407	Easy axis
		4	1.2	8.85	0.04	8.89	2.24	15	443	Easy axis
Experimental										
FePt		...	1.14	6.6	2.00	28.9	406	...
Sm ₂ Co ₁₇		...	0.97	4.2	1.87	21.5	294	...
Nd ₂ Fe ₁₄ B		...	1.28	4.9	1.54	19	512	...
Sm ₂ Fe ₁₇ N ₃		...	1.233	8.6	2.13	35	473	...
SmCo ₅		...	0.88	17.2	4.33	39.1	231	...

In this system, several stable/metastable compounds were predicted. Depending on the value of $U - J$, we found several promising compounds and plotted the ternary convex hull diagram as shown in Fig. 2(d). Among the predicted ternary compounds, we found two promising antiferromagnetic and ferromagnetic phases: WMnB_2 and W_3MnB_4 . Of these, WMnB_2 turned out to be stable at different values of $U - J$ and W_3MnB_4 was found to be metastable with very low energy—for example, 7 meV/atom above the convex hull at $U - J = 0$ eV. Another predicted phase, W_2MnB_2 , is not a promising hard magnet, but it has been experimentally synthesized^{68,69} and our calculations have successfully predicted this compound to be stable at all values of $U - J$. The experimental $P4/mbm$ structure⁶⁸ is found to be stable at $U - J \geq 0.3$ eV (Table II), whereas a new $Immm$ polymorph is stable at $(U - J) < 0.3$ eV. Crystal structures of all ternary compounds, studied in this work, are shown in Fig. 3.

1. W_3MnB_4

The predicted W_3MnB_4 has $Pmm2$ space group [Fig. 3(a)], and theoretically, it exhibits a very large MAE and H_a due to the spin-orbit coupling. Although W_3MnB_4 for all values of $U - J$ has a very large MAE (comparable to rare earth permanent magnets), this compound in pure form is not a good candidate for permanent magnets since it does not have uniaxial anisotropy. However, using techniques such as megajoule magnets^{70,71} (where hard and soft magnets are coupled in a nanostructure composite) or optimization of structure with a fourth element, uniaxial anisotropy and larger energy product can be achieved. We report the relevant magnetic properties for this material in Table II.

2. WMnB_2

The second ternary compound, which shows stability for all values of $(U - J)$, is WMnB_2 . This compound was first predicted with $U - J = 4$ eV, at which value, the stable phase has space group $P2_1/m$. Performing calculations with $(U - J)$ below 3 eV, we found other stable structures. For $U - J = 0$ eV, the stable structure has space group $I\bar{4}m2$; for $U - J = 1$ eV, space group $Pmmm$; and for $U - J = 2$ eV, space group $Amm2$ [Fig. 3(b)]. Experimental synthesis yielded the latter structure, but no magnetization was found.

In structure prediction calculations with up to 16 atoms in the primitive cell, WMnB_2 was found to be stable in the ferromagnetic state. This calculation, however, does not exclude antiferromagnetic solutions with larger cells.⁷² Indeed, susceptibility calculations [Fig. 4(a)] indicated the preference of antiferromagnetic order (supported by explicit calculations of antiferromagnetic ordering and by experiment, see below). If WMnB_2 were ferromagnetic (and perhaps, a ferromagnetic state can be induced by doping or strain), it would be a hard magnet.

3. DMFT for WMnB_2

To explore the magnetic properties of WMnB_2 and to shed light on some of its electronic properties (see the [supplementary material](#)), we consider the electron correlations using the DFT + DMFT approach. For Mn 3d states, we adopt $U = 3$ eV and $J = 0.9$ eV used in previous DMFT studies of γ -Mn,^{73,74} while smaller values of $U = 2.5$ eV and $J = 0.5$ eV were taken for tungsten due to stronger screening in the 5d-elements. Our DMFT calculations explicitly include the 3d, 4s, and 4p states of Mn, 5d and 6s states of

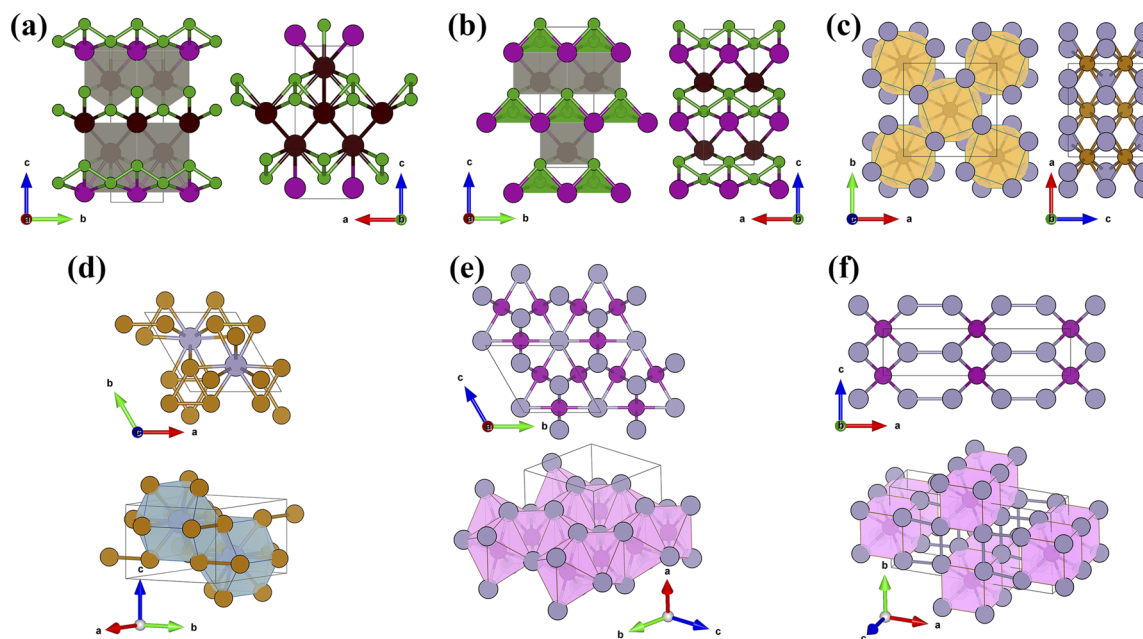


FIG. 3. Crystal structures of studied magnetic systems: (a) $Pmm2 - \text{W}_3\text{MnB}_4$, (b) $Amm2 - \text{WMnB}_2$, (c) $I4/mcm - \text{FeSn}_2$, (d) $P6_3/mmc - \text{Fe}_3\text{Sn}$, (e) $P6/mmm - \text{MnSn}$, (f) $Cmmm - \text{MnSn}_4$. Black atoms correspond to W, purple to Mn, gray to Sn, gold to Fe, and green to B. For better insight, each crystal structure is shown from two views.

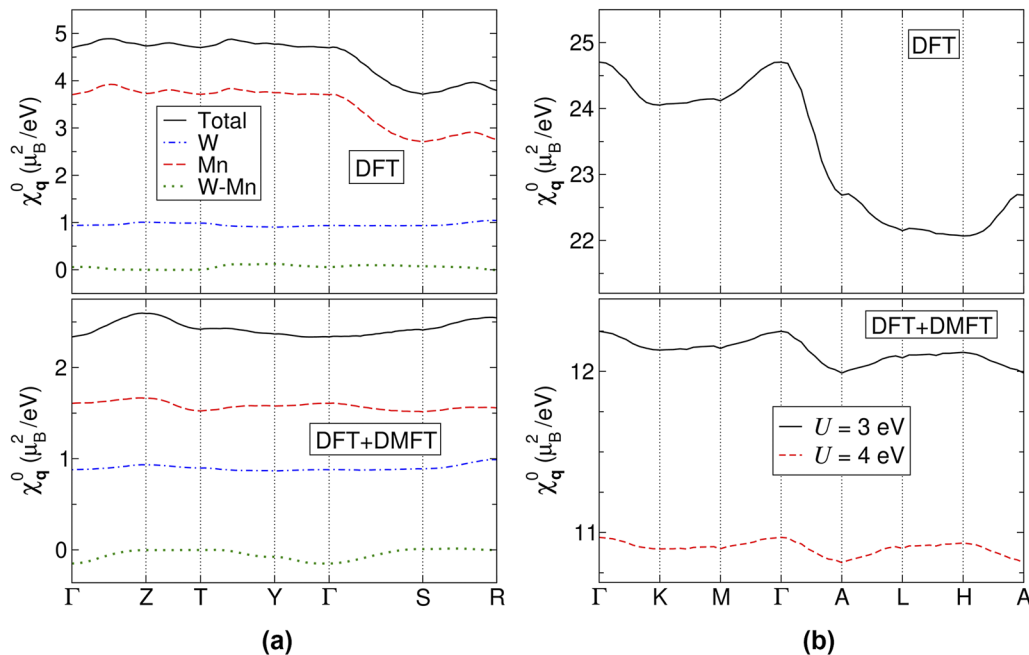


FIG. 4. Momentum-dependent susceptibility of (a) WMnB_2 and (b) Fe_3Sn obtained by DFT and DFT + DMFT at $\beta = 20 \text{ eV}^{-1}$ for WMnB_2 and $\beta = 10 \text{ eV}^{-1}$, different values of Hubbard U and fixed $J = 0.9 \text{ eV}$, for Fe_3Sn . W-Mn corresponds to the mixed inter-site contribution to Eq. (8).

W, $2s$ and $2p$ states of B, by constructing a basis set of site-centered Wannier functions as described in Ref. 75.

Using the DFT-Hamiltonian matrix H_{DFT} in the basis of Wannier functions and the self-energy Σ , obtained in DMFT approach, we calculate the momentum dependence of the magnetic susceptibility in the zeroth order in the interaction vertices (particle-hole bubble),

$$\chi_{\mathbf{q}}^0 = -(2\mu_B^2/\beta) \sum_{\mathbf{k}, \nu_n, ij, mm'} G_{\mathbf{k}}^{im, jm'}(i\nu_n) G_{\mathbf{k}+\mathbf{q}}^{j'm', im}(i\nu_n), \quad (8)$$

where $\beta = 1/T$ is the inverse temperature, $G_{\mathbf{k}}(i\nu_n)^{im, jm'} = [(\mu + i\nu_n)I - H_{\text{DFT}}(\mathbf{k}) - \Sigma(i\nu_n)]_{im, jm'}^{-1}$ is the one-particle Green's function for wave vector \mathbf{k} and fermionic Matsubara frequency $\nu_n = (2n + 1)\pi/\beta$, μ is the chemical potential, I is the unit matrix, i and j are site indices, and m and m' are orbital indices. We have verified the convergence of the obtained results with respect to the density of the grid in momentum space. The obtained $\chi_{\mathbf{q}}^0$ is shown in Fig. 4(a). One can see that in DFT ($\Sigma = 0$), the maximum of the particle-hole bubble is achieved for the incommensurate wave vectors in $\Gamma - Z$ and $\Gamma - Y$ directions. Near these maxima, the bubble is characterized by rather weak momentum dependence, such that close competition between ferromagnetic and these incommensurate correlations is expected. At the same time, in DMFT, we find stronger momentum dependence of the particle-hole bubble, with the maxima, located at wave vectors, corresponding to the Z and R points of the Brillouin zone. Therefore, according to these DMFT results, the antiferromagnetic order with the above-mentioned wave vectors is expected to be dominant.

4. Synthesis of WMnB_2

There have been very few studies focusing on the W-Mn-B system, mostly in 1960–1970s.^{68,69,76} The latest of these works⁶⁹ concludes that the following ternary compounds are stable: $(\text{W}, \text{Mn})_3\text{B}_2$ (U_3Si_2 -type structure), W_4MnB_5 (CrB-type structure with homogeneity region 38–42 at.% W, 8–12 at.% Mn), and WMnB with unknown structure. Our calculations, however, predict that WMnB_2 should be stable as well, and we decided to test this prediction experimentally.

This compound was indeed synthesized. In order to determine precisely the structure of WMnB_2 , the structure of recovered pellet samples from high-pressure experiments (see the [supplementary material](#)) was studied by powder x-ray diffraction using an Equinox 1000 Inel diffractometer (Bragg-Brentano geometry, Cu $K\alpha$ radiation). The lattice parameters have been derived from the Le Bail profile refinement procedure⁷⁷ performed using the PowderCell software. The characteristic diffraction pattern of the single-phase WMnB_2 sample is shown in Fig. 5(b). The lattice parameters are $a = 3.012(2) \text{ \AA}$, $b = 3.120(1) \text{ \AA}$, and $c = 8.130(8) \text{ \AA}$ (in the $\text{Amm}2$ setting), or $a = 3.120(1) \text{ \AA}$, $b = 8.130(8) \text{ \AA}$, and $c = 3.012(2) \text{ \AA}$ (in the Cmcm setting), in excellent agreement with the above-described experiment and with theoretical prediction. The only difference is that our predicted structure is fully ordered (and has lower space group $\text{Amm}2$), whereas in experiment (due to high temperatures of synthesis), the same crystal structure was obtained, but with W-Mn disorder (hence higher symmetry— Cmcm).

Measurements of magnetization indicate that WMnB_2 is not a ferromagnet in its ground state. The shape of the hysteresis

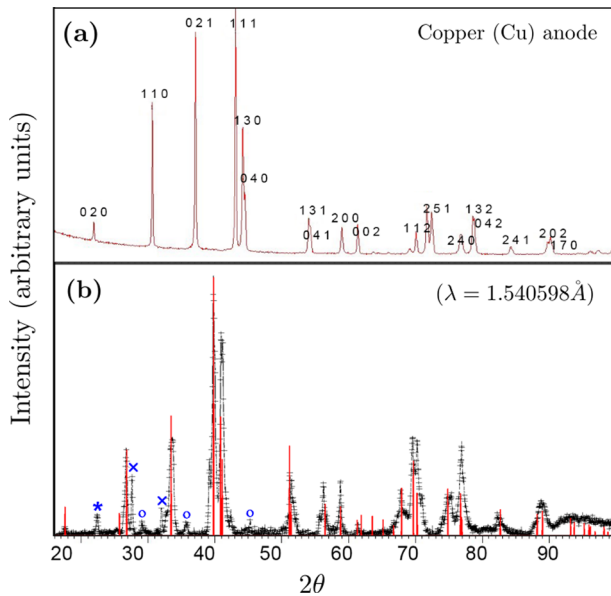


FIG. 5. (a) X-ray diffraction pattern showing 100% yield of WMnB_2 . (b) X-ray diffraction pattern of WMnB_2 synthesized at 5.2 GPa and 2500 K. Vertical red ticks correspond to expected positions and intensities of diffraction lines of the orthorhombic $Amm2$ structure predicted with $U - J = 2$ eV. Blue asterisk, crosses, and circles correspond to graphite, WC ($P\bar{6}m2$), and WB ($I4_1/amd$) impurities, respectively.

loop [Fig. 6(b)] is not typical of an antiferromagnet either, and we think that this material has both ferromagnetic and antiferromagnetic interactions and is closer to the antiferromagnetic state. At 2 K in fields $H > 30$ –40 kOe, there is a difference between the ZFC curve and the field-down branch of the hysteresis loop, which indicates a strong magnetic anisotropy in the antiferromagnetic state. Nonlinearity of $M(H)$ is strongest at low temperatures, while the magnetization curves are close to linear at temperatures above 100 K. Both the coercivity H_c and remanence M_r decrease fast with increasing temperature [Fig. 6(c)]. Temperature dependence

of the derivative $dM(T)/dT$ shows two possible phase transitions: one at 50 K and the other at 200 K [inset in Fig. 6(c)]. At 50 K, we observe the disappearance of hysteresis; but, according to the magnetic susceptibility data, ferromagnetic and antiferromagnetic interactions persist at higher temperatures. The anomaly at 200 K is likely due to the Néel transition from the antiferromagnetic to the paramagnetic state (which, however, still has small parasitic ferromagnetism).

D. Fe–Sn system

Alongside ternary systems, we also explored two binary systems, viz., Fe–Sn and Mn–Sn, where tin is a heavy metal needed for strong spin–orbit coupling and iron/manganese are donors of the spin density. We searched for low-energy structures of these systems using the evolutionary algorithm USPEX for 60 generations (by exploring around 5000 structures with different stoichiometries). Details of *ab initio* calculations are similar to W–Mn–B calculations and are explained in Sec. III C. In these calculations, several promising stable and low-energy metastable structures were found at different $U - J$ —see the convex hull diagram of the Fe–Sn system in Fig. 2(b).

For $U - J = 0$ eV, it turned out that two compounds FeSn_2 and Fe_3Sn_2 are stable, while there are no other metastable compounds close to the convex hull. Fe_3Sn_2 was found to be stable at all values of $U - J$, and its crystal structure is known experimentally to be $R\bar{3}m$,⁷⁸ which is in agreement with our prediction for $(U - J) < 1.8$ eV. Our calculations predict Fe_3Sn_2 to be a ferromagnet (in agreement with experiment^{79,80}), but the calculated MAE for all $U - J$ is at least an order of magnitude larger than the experimental value.^{79,80} At $U - J = 1$ eV, several metastable compounds were predicted, while none of them showed the properties of a hard magnet.

Similarly, several metastable compounds, such as Fe_7Sn , Fe_6Sn , Fe_8Sn , Fe_5Sn , and Fe_4Sn , were found at $U - J = 2$ eV. Our calculations show that at $U - J = 2$ eV, Fe_3Sn is a promising hard magnet candidate. Of the metastable compounds, Fe_4Sn turned out to be antiferromagnetic and Fe_8Sn , Fe_7Sn , Fe_5Sn , and Fe_6Sn were found to have a very low anisotropy constant. (For more details on the structures of these compounds, see the [supplementary material](#).)

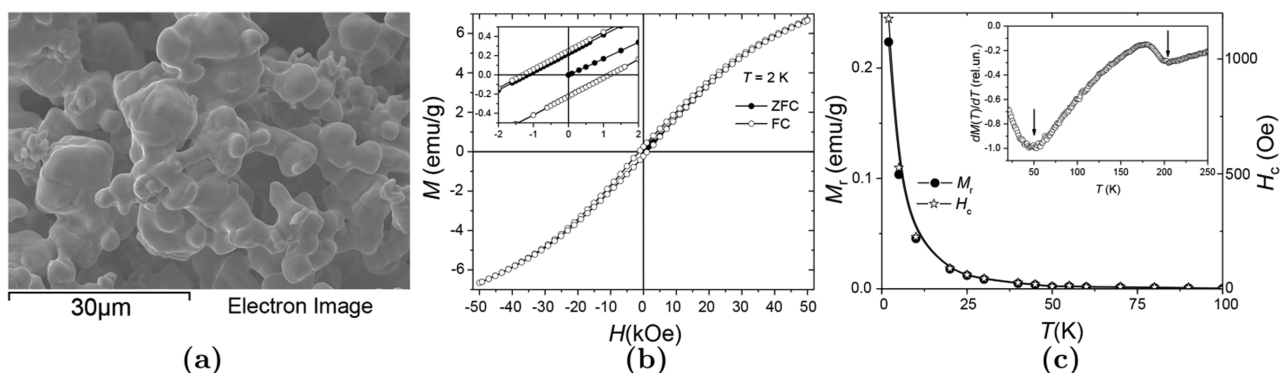


FIG. 6. (a) Sample under electron microscope ($\times 3000$). (b) Isotherms $M(H)$ of WMnB_2 at $T = 2$ K. Sample was cooled from $T = 300$ K down to 2 K, at which temperature the magnetization curve was measured [zero field cooling (ZFC) was done at $H \approx -8$ Oe, field cooling (FC) at $H = 50$ kOe]. (c) Temperature dependence of the remanence M_r and coercivity H_c of WMnB_2 . Inset: temperature dependence of the derivative $dM(T)/dT$. The arrows correspond to the expected magnetic phase transition temperatures.

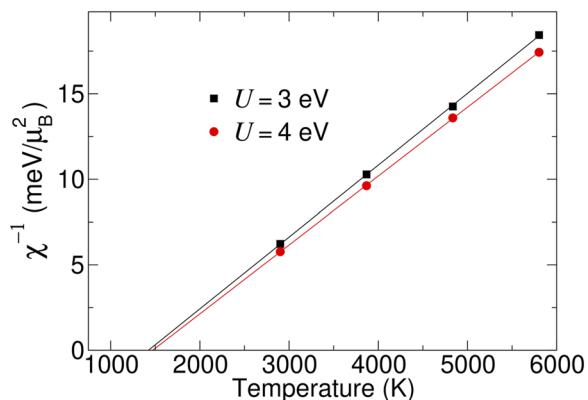


FIG. 7. Inverse uniform magnetic susceptibility of Fe_3Sn as a function of temperature obtained by DFT + DMFT with different values of Hubbard U and fixed $J = 0.9$ eV.

1. FeSn_2

For FeSn_2 with $U - J = 0$ eV, we found metastable phases with space groups $I4/m$, $P1$, $C2/c$, $C2/m$ and a stable phase with space group $I4/mcm$. The stable phase also shows interesting hard magnet properties, and its crystal structure is in excellent agreement with the experimental data (Table II). Our prediction of the MAE for this phase is 1.88 MJ/m^3 with easy plane anisotropy, which is not desirable for permanent magnets; its crystal structure is shown in Fig. 3(c). This phase can be studied more in regard to whether an easy axis anisotropy is achievable or not and how to improve the

energy product by adding a third element to increase magnetization. Other properties of this phase are listed in Table II.

2. Fe_3Sn

This compound has two competitive structures, both with space group $P6_3/mmc$: one with two and the other with four formula units in the unit cell. Here, we study the former structure as it has higher magnetization and is stable at $U - J = 2$ eV [Fig. 3(d)]. This phase is stabilized by on-site electron correlation and it is stable only at $U - J > 1.7$ eV. The structure of this phase is again in good agreement with experimental results (Table II). Previous DFT calculations and experimental result⁸⁰ have shown that this compound has a large MAE of 1.59 MJ/m^3 , but here we performed the DFT + U calculation of MAE with $U - J = 0$ and 2 eV. Interestingly, the MAE we calculated for $U - J = 0$ ($\approx 1.1 \text{ MJ/m}^3$) is of the same order as the result of [80], but our calculations show that Fe_3Sn is a thermodynamically metastable phase at $U - J = 0$ (it is 0.035 eV/atom above the convex hull); on the other hand, for the stable phase with $U - J = 2$ eV, our calculations show that Fe_3Sn has negligible MAE ($\approx 0.16 \text{ MJ/m}^3$) but large $|BH|_{\text{MAX}}$, up to 545 KJ m^{-3} for the stable phase with an easy axis anisotropy. This means for $P6_3/mmc$ - Fe_3Sn , increasing $U - J$ would stabilize the structure but worsen the hard magnetic properties.

For further insight into the magnetic properties of Fe_3Sn , we take into account the electron correlations using the DFT + DMFT approach. We use $U = 3$ eV and $J = 0.9$ eV, which are in agreement with previously obtained estimates for elemental iron.⁸¹ We also consider larger $U = 4$ eV to make sure that our choice of the $U - J$ parameter does not qualitatively affect the results. In our DMFT calculations, we explicitly include the $3d$, $4s$, and $4p$ states of Fe and $5s$,

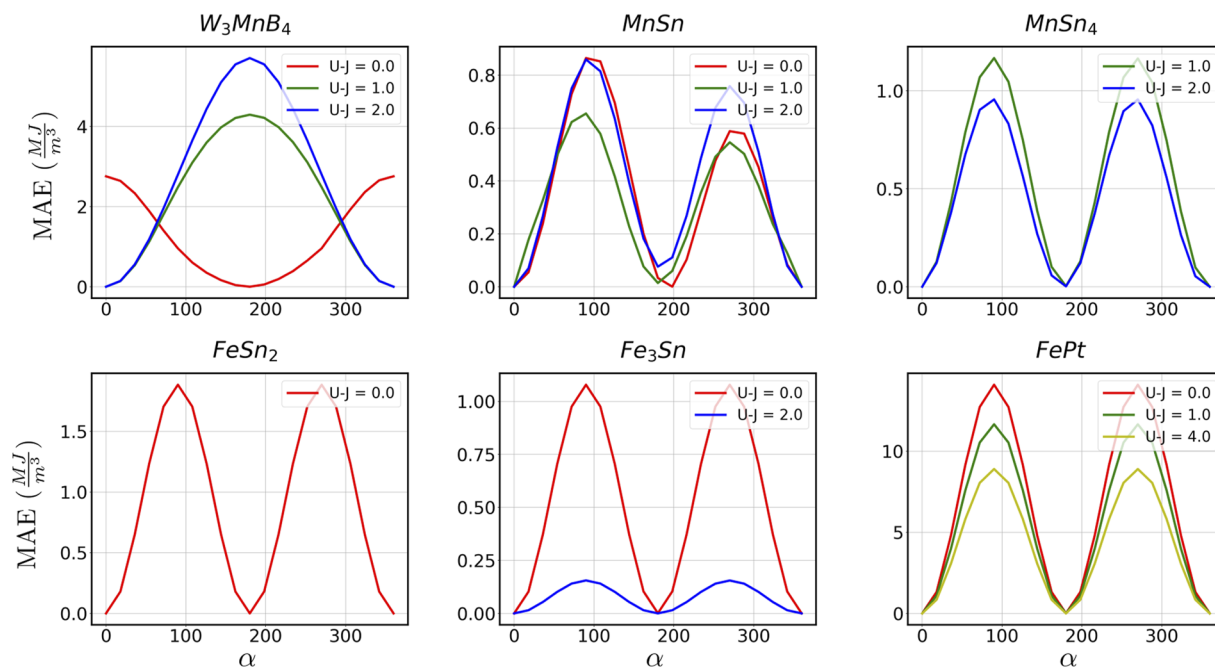


FIG. 8. MAE curves for each stable phase and different $U - J$ values.

5p states of Sn, by constructing a basis set of site-centered Wannier functions as described in Ref. 75.

In Fig. 4(b), we present the momentum dependence of the particle-hole bubble χ_q^0 calculated by Eq. (8). In DFT, we find clear peaks of the particle-hole bubble at $\mathbf{q} = 0$, showing that ferromagnetism is expected to be the dominant mode of instability for this compound. The peaks of the particle-hole bubble at the Γ point are also preserved in DFT + DMFT analysis, which yields, however, closer competition of the obtained ferromagnetic order with spin-density-wave correlations, characterized by the wave vector \mathbf{q}_H .

Next, we calculate the uniform magnetic susceptibility as a response to a small external field introduced in the DMFT part. We find (see Fig. 7) a linear temperature dependence of inverse susceptibility with the theoretical Curie temperature $T_C \approx 1500$ K, which weakly depends on Hubbard U . At present, most material-specific DMFT calculations consider the Coulomb interaction in

the density-density form, which corresponds to the Ising symmetry of Hund's exchange. This approximation drastically reduces the computational cost, making such calculations feasible. However, it leads to an overestimation of the Curie temperature.⁸² Moreover, the mean-field nature of DMFT also contributes to the overestimation of Curie temperature, which can only be overcome by sophisticated approaches beyond DMFT. Previous DFT + DMFT studies of metallic iron found that the two above-mentioned approximations lead to about twofold overestimation of its Curie temperature.^{81,83} Assuming the same ratio of calculated and experimental Curie temperatures, we obtain a rough estimate of the Curie temperature for Fe₃Sn to be ~ 750 K, which is very close to the experimentally measured $T_c = 725$ K.⁸⁰

E. Mn-Sn system

The thermodynamic convex hulls for the Mn-Sn system for all ($U - J$) values are shown in Fig. 2(c). In this system, there are multi-

TABLE III. DFT energies of formation, space groups, and optimized lattice parameters from our calculations and available experiments (full information about structural properties and energies is provided in the [supplementary material](#)).

Compound	Space group	$(U - J)$ (eV)		Lattice parameters for selected $(U - J)$				ΔH_f (eV/atom)
		Range of stability	a (Å)	b (Å)	c (Å)	β (deg)	$(U - J)$ (eV)	
W ₂ MnB ₂	<i>I</i> mmm	$0.0 \leq U - J < 0.3$	3.120	4.668	7.200	...	0	-0.492
W ₂ MnB ₂	<i>P</i> ₄ /mbm	$0.3 \leq U - J$	5.812	5.812	3.176	...	1	-0.522
W ₂ MnB ₂	<i>P</i> ₄ /mbm		5.786	5.786	3.160	...	EXP ⁶⁹	
W ₃ MnB ₄	<i>P</i> mm2	...	3.145	3.070	8.289	...	0	-0.484
W ₃ MnB ₄	<i>P</i> mm2	...	3.159	3.076	8.329	...	1	-0.510
W ₃ MnB ₄	<i>P</i> mm2	...	3.158	3.076	8.329	...	2	-0.468
WMnB ₂	$\bar{I}4m2$	$0.0 \leq U - J \leq 0.9$	3.069	3.069	16.063	...	0	-0.538
WMnB ₂	<i>P</i> mmn	$0.9 < U - J \leq 1.6$	3.047	3.104	7.979	...	1	-0.566
WMnB ₂	<i>A</i> mm2	$1.6 < U - J$	3.017	3.104	8.128	...	2	-0.449
WMnB ₂	<i>A</i> mm2		3.012	3.120	8.130	...	[EXP, this work]	
W ₂ Mn ₃ B ₂	<i>A</i> 2/ <i>m</i>	$0.0 \leq U - J < 0.9$	8.645	2.940	6.296	112	0	-0.412
W ₂ Mn ₃ B ₂	<i>A</i> 2/ <i>m</i>	$0.9 \leq U - J < 1.5$	8.513	3.136	5.767	81	1	-0.425
FeSn ₂	<i>I</i> 4/ <i>mcm</i>	$0.0 \leq U - J \leq 0.4$	6.559	6.559	5.326	...	0	-0.0065
FeSn ₂	<i>I</i> 4/ <i>mcm</i>		6.533	6.533	5.323	...	EXP ⁸⁵	
Fe ₃ Sn	<i>P</i> 6 ₃ / <i>mmc</i>	$1.7 < U - J$	5.522	5.522	4.344	...	2	-0.0159
Fe ₃ Sn	<i>P</i> 6 ₃ / <i>mmc</i>		5.464	5.464	4.352	...	EXP ⁸⁶	
Fe ₃ Sn ₂	$\bar{R}3m$	$0.0 \leq U - J \leq 1.7$	5.326	5.326	19.803	...	0	-0.0174
Fe ₃ Sn ₂	$\bar{R}3m$		5.344	5.344	19.797	...	EXP ⁷⁸	
MnSn	<i>P</i> 6/ <i>mmm</i>	...	5.389	5.389	4.478	...	0	-0.0560
MnSn	<i>P</i> 6/ <i>mmm</i>	...	5.411	5.411	4.546	...	1	-0.0925
MnSn	<i>P</i> 6/ <i>mmm</i>	...	5.680	5.680	4.780	...	2	-0.0775
MnSn ₄	<i>C</i> mmm	$0.7 \leq U - J$	12.678	6.422	3.131	...	1	-0.0423
MnSn ₄	<i>C</i> mmm		12.763	6.502	3.156	...	2	-0.0507
MnSn ₂	<i>I</i> 4/ <i>mcm</i>	$0.6 \leq U - J$	6.725	6.725	5.528	...	1	-0.067
MnSn ₂	<i>I</i> 4/ <i>mcm</i>		6.671	6.671	5.443	...	EXP ⁸⁷	

ple stable and metastable phases, some of which we show to be good candidates candidate for permanent magnet production. Among the predicted phases, MnSn_2 (an experimentally synthesized phase in the Mn–Sn system) is stable at $0.6 \text{ eV} \leq U - J$ and its crystal structure is correctly predicted in our calculations (Table II); however, this compound is not a promising hard magnet. Below, we report on two promising hard magnet candidates with easy axis anisotropy for some values of $U - J$.

1. MnSn

This phase has space group $P6/mmm$ [Fig. 3(f)] and is stable at all values of $(U - J)$ explored here. For $U - J = 0 \text{ eV}$, this phase has an easy axis anisotropy, but for $U - J = 1, 2 \text{ eV}$, it has easy plane anisotropy. MnSn has a reasonably good value of anisotropy field and MAE compared to rare earth hard magnets, suggesting this phase can be a good candidate for a cheap hard magnet. MnSn shows the largest spontaneous magnetization among all compounds studied in this work (comparable to Sm–Co hard magnets). For other magnetic properties of this phase, see Table II.

2. MnSn_4

This compound showed stability when we included the U -correction in our calculations. Its structure [Fig. 3(g)] has space group $Cmmm$. For both $U - J = 1$ and $U - J = 2$, this phase has an easy axis anisotropy with a large anisotropy field and a rather high MAE, but a small spontaneous magnetization makes its energy product the lowest among all the studied phases.

Our results show that systems containing Mn have large MAE, see the MAE curve for each selected material in Fig. 8 and the calculated magnetic properties are collected in Table II and can be compared with those of state-of-the-art hard magnets. The lattice parameters of selected compounds and available experimental values are provided in Table III. Moreover, $(U - J)$ -composition phase diagrams of the Fe–Sn, Mn–Sn, and W–Mn–B systems and details of crystal structure and magnetic moments are provided in the supplementary material.

IV. CONCLUSIONS

Experiments involving magnetic materials are challenging for several reasons. First, multiple magnetic structures are very close in energy and cannot be exhaustively sampled in many cases. Second, standard DFT calculations are often too crude, and DFT + U is only semiquantitative. Here, we show how a simple extension of the evolutionary algorithm USPEX allowed us to optimize the magnetic structure together with atomic structure and chemical composition. Detailed DFT + DMFT calculations and experiments can then be performed for the most interesting predicted materials. A new function for quantifying the half-metallicity of a material is proposed and several low-energy half-metallic phases are predicted in the Cr–O system using multi-objective Pareto optimization as implemented in the evolutionary algorithm USPEX. Using USPEX, we searched for stable phases with high magnetization. Thereafter, promising predicted systems were studied more thoroughly. Our aim is to discover materials with high energy product $|BH|_{\text{MAX}}$ as well as high anisotropy field H_a . For example, our results show high value of $|BH|_{\text{MAX}}$ for Fe_3Sn and MnSn (due to high magnetization

M_0), and high anisotropy field in Mn-rich phases. In the studied systems (i.e., W–Mn–B, Fe–Sn and Mn–Sn), our calculations recovered all experimentally known compounds and crystal structures and resulted in a number of new predictions, also checking if larger-cell magnetic ordering exists. One of the newly predicted materials, antiferromagnetic WMnB_2 has been confirmed by direct experimental synthesis.

In total, we predicted five magnetic materials in our USPEX calculations. Two of them, Fe_3Sn and MnSn , theoretically, have shown high $|BH|_{\text{MAX}}$ and rather high anisotropy field, comparable to that of available hard magnets, and the values exceed or are comparable to those of other theoretically predicted compounds with no rare earth elements;^{88–90} thus, they are of potential technological interest. W_3MnB_4 has also shown high anisotropy field, but its relatively low energy product is a drawback. In short, we can say that our method has shown great efficacy, and the goal of finding rare earth-free hard magnets appears achievable. The main current limitation is the imperfect description of such systems by both DFT and DFT + U approaches. Exploring ranges of $(U - J)$ values and building “correlation phase diagram” gives a variety of possible solutions (see the supplementary material). There is an ongoing debate as to how to model electron correlations in magnetic materials in order to obtain reliable results cheaply. Even within the DFT + U approach, recent studies have shown that varying U and J separately is more reliable than only using their difference.⁹¹ Irrespective of which way of modeling electron correlations is superior, our work describes a framework that can be used in conjunction with any method for calculating magnetic properties, and as the accuracy of such methods improves, the prediction of novel magnetic materials within our approach will become more and more accessible.

CODE AVAILABILITY

The extension of USPEX to magnetic materials is publicly available. The extension of USPEX to half-metals will be available in the subsequent release.

SUPPLEMENTARY MATERIAL

The supplementary material contains details of half-metallicity, MAE convergence, DMFT calculation of electronic structure, experimental setup, and information about stable/metastable crystal structures.

ACKNOWLEDGMENTS

The theoretical study of ferromagnets and DFT + DMFT calculations were supported by the Russian Science Foundation (Grant No. 19-72-30043). We thank Dr. V. A. Mukhanov for assistance in high-pressure experiments and I. V. Blinov, P. Y. Plechov, and A. N. Vasilyev for their help in the initial stages of this project.

AUTHOR DECLARATIONS

Conflict of Interest

The authors have no conflicts to disclose.

Author Contributions

S. Rahmanian Koshkaki and Z. Allahyari contributed equally to this work.

Saeed Rahmanian Koshkaki: Conceptualization (equal); Data curation (equal); Formal analysis (equal); Investigation (equal); Methodology (equal); Project administration (equal); Software (equal); Validation (equal); Visualization (equal); Writing – original draft (equal); Writing – review & editing (equal). **Guang-Rui Qian:** Conceptualization (supporting); Investigation (supporting); Methodology (supporting); Software (supporting); Validation (supporting). **Konstantin V. Maksimtsev:** Conceptualization (supporting); Data curation (supporting); Formal analysis (supporting); Investigation (supporting); Methodology (supporting); Validation (supporting); Visualization (supporting); Writing – original draft (supporting). **Andrey S. Mukhamadeev:** Conceptualization (supporting); Data curation (supporting); Formal analysis (supporting); Investigation (supporting); Methodology (supporting); Validation (supporting); Visualization (supporting); Writing – original draft (supporting). **Andrey V. Chukin:** Conceptualization (supporting); Data curation (supporting); Formal analysis (supporting); Investigation (supporting); Methodology (supporting); Validation (supporting); Visualization (supporting); Writing – original draft (supporting). **Aleksandr V. Korolev:** Conceptualization (supporting); Data curation (supporting); Formal analysis (supporting); Investigation (supporting); Methodology (supporting); Validation (supporting); Visualization (supporting); Writing – original draft (supporting). **Nikolay V. Mushnikov:** Conceptualization (supporting); Data curation (supporting); Formal analysis (supporting); Investigation (supporting); Methodology (supporting); Resources (supporting); Validation (supporting); Writing – original draft (supporting). **Hao Li:** Data curation (supporting); Methodology (supporting); Software (supporting); Validation (supporting). **Zahed Allahyari:** Conceptualization (equal); Data curation (equal); Formal analysis (equal); Investigation (equal); Methodology (equal); Project administration (equal); Software (equal); Validation (equal); Visualization (equal); Writing – original draft (equal); Writing – review & editing (equal). **Artem R. Oganov:** Conceptualization (equal); Formal analysis (equal); Funding acquisition (lead); Investigation (equal); Methodology (equal); Resources (lead); Software (equal); Supervision (lead); Validation (lead); Writing – original draft (equal); Writing – review & editing (equal). **Vladimir L. Solozhenko:** Conceptualization (supporting); Formal analysis (supporting); Investigation (supporting); Methodology (supporting); Validation (supporting); Writing – original draft (supporting). **Ilya B. Polovov:** Conceptualization (supporting); Data curation (supporting); Formal analysis (supporting); Investigation (supporting); Methodology (supporting); Supervision (supporting); Validation (supporting); Visualization (supporting); Writing – original draft (supporting). **Alexander S. Belozerov:** Conceptualization (supporting); Data curation (supporting); Formal analysis (supporting); Investigation (equal); Methodology (supporting); Software (equal); Validation (supporting); Visualization (supporting); Writing – original draft (supporting). **Andrey A. Katanin:** Conceptualization (supporting); Data curation (supporting); Formal analysis (supporting); Investigation (equal); Methodology (supporting); Software (equal); Validation (supporting); Visualization (supporting); Writing – original draft

(supporting). **Vladimir I. Anisimov:** Conceptualization (supporting); Data curation (supporting); Formal analysis (supporting); Investigation (supporting); Methodology (supporting); Software (supporting); Supervision (supporting); Validation (supporting); Visualization (supporting); Writing – original draft (supporting). **Evgeny V. Tikhonov:** Conceptualization (supporting); Data curation (supporting); Formal analysis (supporting); Methodology (supporting); Validation (supporting).

DATA AVAILABILITY

The data that support the findings of this study are available from the corresponding author upon reasonable request.

REFERENCES

- ¹K. Strnat, “The recent development of permanent magnet materials containing rare earth metals,” *IEEE Trans. Magn.* **6**, 182–190 (1970).
- ²S. D. Bader and S. S. P. Parkin, “Spintronics,” *Annu. Rev. Condens. Matter Phys.* **1**, 71–88 (2010).
- ³S. A. Wolf, A. Y. Chtchelkanova, and D. M. Treger, “Spintronic – A retrospective and perspective,” *IBM J. Res. Dev.* **50**, 101–110 (2006).
- ⁴J. M. D. Coey, “Hard magnetic materials: A perspective,” *IEEE Trans. Magn.* **47**, 4671–4681 (2011).
- ⁵A. R. Oganov *et al.*, *Computational Materials Discovery* (Royal Society of Chemistry, 2018).
- ⁶A. R. Oganov, C. J. Pickard, Q. Zhu, and R. J. Needs, “Structure prediction drives materials discovery,” *Nat. Rev. Mater.* **4**, 331–348 (2019).
- ⁷S. Curtarolo *et al.*, “The high-throughput highway to computational materials design,” *Nat. Mater.* **12**, 191–201 (2013).
- ⁸A. R. Oganov and C. W. Glass, “Crystal structure prediction using *ab initio* evolutionary techniques: Principles and applications,” *J. Chem. Phys.* **124**, 244704 (2006).
- ⁹A. O. Lyakhov, A. R. Oganov, H. T. Stokes, and Q. Zhu, “New developments in evolutionary structure prediction algorithm USPEX,” *Comput. Phys. Commun.* **184**, 1172–1182 (2013).
- ¹⁰Z. Allahyari and A. R. Oganov, “Coevolutionary search for optimal materials in the space of all possible compounds,” *npj Comput. Mater.* **6**, 1–10 (2020).
- ¹¹Zhao *et al.*, “Exploring the structural complexity of intermetallic compounds by an adaptive genetic algorithm,” *Phys. Rev. Lett.* **112**, 045502 (2014).
- ¹²A. Halder, D. Nafday, P. Sanyal, and T. Saha-Dasgupta, “Computer predictions on Rh-based double perovskites with unusual electronic and magnetic properties,” *npj Quantum Mater.* **3**, 1–8 (2018).
- ¹³A. R. Oganov, Y. Ma, A. O. Lyakhov, M. Valle, and C. Gatti, “Evolutionary crystal structure prediction as a method for the discovery of minerals and materials,” *Rev. Mineral. Geochem.* **71**, 271–298 (2010).
- ¹⁴A. R. Oganov, A. O. Lyakhov, and M. Valle, “How evolutionary crystal structure prediction works—and why,” *Acc. Chem. Res.* **44**, 227–237 (2011).
- ¹⁵J. P. Perdew, K. Burke, and M. Ernzerhof, “Generalized gradient approximation made simple,” *Phys. Rev. Lett.* **77**, 3865–3868 (1996).
- ¹⁶A. I. Liechtenstein, V. I. Anisimov, and J. Zaanen, “Density-functional theory and strong interactions: Orbital ordering in Mott-Hubbard insulators,” *Phys. Rev. B* **52**, R5467–R5470 (1995).
- ¹⁷S. L. Dudarev, G. A. Botton, S. Y. Savrasov, C. J. Humphreys, and A. P. Sutton, “Electron-energy-loss spectra and the structural stability of nickel oxide: An LSDA+U study,” *Phys. Rev. B* **57**, 1505–1509 (1998).
- ¹⁸A. G. Kvashnin, A. R. Oganov, A. I. Samtsevich, and Z. Allahyari, “Computational search for novel hard chromium-based materials,” *J. Phys. Chem. Lett.* **8**, 755–764 (2017).
- ¹⁹Q. Zhu, L. Li, A. R. Oganov, and P. B. Allen, “Evolutionary method for predicting surface reconstructions with variable stoichiometry,” *Phys. Rev. B* **87**, 195317 (2013).
- ²⁰V. Sharma *et al.*, “Rational design of all organic polymer dielectrics,” *Nat. Commun.* **5**, 4845 (2014).

- ²¹C.-H. Hu *et al.*, “Pressure-induced stabilization and insulator-superconductor transition of BH,” *Phys. Rev. Lett.* **110**, 165504 (2013).
- ²²W. Zhang *et al.*, “Unexpected stable stoichiometries of sodium chlorides,” *Science* **342**, 1502–1505 (2013).
- ²³X.-F. Zhou, A. R. Oganov, G.-R. Qian, and Q. Zhu, “First-principles determination of the structure of magnesium borohydride,” *Phys. Rev. Lett.* **109**, 245503 (2012).
- ²⁴G.-R. Qian, A. O. Lyakhov, Q. Zhu, A. R. Oganov, and X. Dong, “Novel hydrogen hydrate structures under pressure,” *Sci. Rep.* **4**, 5606 (2014).
- ²⁵G. Kresse and J. Hafner, “*Ab initio* molecular dynamics for liquid metals,” *Phys. Rev. B* **47**, 558–561 (1993).
- ²⁶G. Kresse and J. Hafner, “*Ab initio* molecular-dynamics simulation of the liquid-metal–amorphous-semiconductor transition in germanium,” *Phys. Rev. B* **49**, 14251–14269 (1994).
- ²⁷G. Kresse and J. Furthmüller, “Efficiency of *ab-initio* total energy calculations for metals and semiconductors using a plane-wave basis set,” *Comput. Mater. Sci.* **6**, 15–50 (1996).
- ²⁸G. Kresse and J. Furthmüller, “Efficient iterative schemes for *ab initio* total-energy calculations using a plane-wave basis set,” *Phys. Rev. B* **54**, 11169–11186 (1996).
- ²⁹V. I. Anisimov, J. Zaanen, and O. K. Andersen, “Band theory and Mott insulators: Hubbard *U* instead of Stoner *I*,” *Phys. Rev. B* **44**, 943–954 (1991).
- ³⁰V. I. Anisimov, I. V. Solovyev, M. A. Korotin, M. T. Czyżyk, and G. A. Sawatzky, “Density-functional theory and NiO photoemission spectra,” *Phys. Rev. B* **48**, 16929–16934 (1993).
- ³¹I. V. Solovyev, P. H. Dederichs, and V. I. Anisimov, “Corrected atomic limit in the local-density approximation and the electronic structure of *d* impurities in Rb,” *Phys. Rev. B* **50**, 16861–16871 (1994).
- ³²B. Himmetoglu, A. Floris, S. de Gironcoli, and M. Cococcioni, “Hubbard-corrected DFT energy functionals: The LDA+*U* description of correlated systems,” *Int. J. Quantum Chem.* **114**, 14–49 (2014).
- ³³W. Metzner and D. Vollhardt, “Correlated lattice fermions in $d = \infty$ dimensions,” *Phys. Rev. Lett.* **62**, 324–327 (1989).
- ³⁴A. Georges, G. Kotliar, W. Krauth, and M. J. Rozenberg, “Dynamical mean-field theory of strongly correlated fermion systems and the limit of infinite dimensions,” *Rev. Mod. Phys.* **68**, 13–125 (1996).
- ³⁵V. I. Anisimov, A. I. Poteryaev, M. A. Korotin, A. O. Anokhin, and G. Kotliar, “First-principles calculations of the electronic structure and spectra of strongly correlated systems: Dynamical mean-field theory,” *J. Phys.: Condens. Matter* **9**, 7359–7367 (1997).
- ³⁶G. Kotliar *et al.*, “Electronic structure calculations with dynamical mean-field theory,” *Rev. Mod. Phys.* **78**, 865–951 (2006).
- ³⁷V. Anisimov and Y. Izyumov *Electronic Structure of Strongly Correlated Materials* (Springer, 2010).
- ³⁸Advanced materials simulation Ekaterinburg’s toolbox, <http://amulet-code.org>.
- ³⁹V. I. Anisimov, F. Aryasetiawan, and A. I. Lichtenstein, “First-principles calculations of the electronic structure and spectra of strongly correlated systems: The LDA + *U* method,” *J. Phys.: Condens. Matter* **9**, 767–808 (1997).
- ⁴⁰A. V. Krukau, O. A. Vydrov, A. F. Izmaylov, and G. E. Scuseria, “Influence of the exchange screening parameter on the performance of screened hybrid functionals,” *J. Chem. Phys.* **125**, 224106 (2006).
- ⁴¹J. Heyd, G. E. Scuseria, and M. Ernzerhof, “Hybrid functionals based on a screened Coulomb potential,” *J. Chem. Phys.* **118**, 8207–8215 (2003).
- ⁴²W. Jia *et al.*, “The analysis of a plane wave pseudopotential density functional theory code on a GPU machine,” *Comput. Phys. Commun.* **184**, 9–18 (2013).
- ⁴³W. Jia *et al.*, “Fast plane wave density functional theory molecular dynamics calculations on multi-GPU machines,” *J. Comput. Phys.* **251**, 102–115 (2013).
- ⁴⁴J. Harris, “Simplified method for calculating the energy of weakly interacting fragments,” *Phys. Rev. B* **31**, 1770–1779 (1985).
- ⁴⁵R. Skomski *et al.*, *Simple Models of Magnetism* (Oxford University Press on Demand, 2008).
- ⁴⁶J. M. D. Coey and S. Sanvito, “Magnetic semiconductors and half-metals,” *J. Phys. D: Appl. Phys.* **37**, 988–993 (2004).
- ⁴⁷R. Shan *et al.*, “Demonstration of half-metallicity in fermi-level-tuned Heusler alloy $\text{Co}_2\text{FeAl}_{0.5}\text{Si}_{0.5}$ at room temperature,” *Phys. Rev. Lett.* **102**, 246601 (2009).
- ⁴⁸M. I. Katsnelson, V. Y. Irkhin, L. Chioncel, A. I. Lichtenstein, and R. A. de Groot, “Half-metallic ferromagnets: From band structure to many-body effects,” *Rev. Mod. Phys.* **80**, 315–378 (2008).
- ⁴⁹R. A. de Groot, F. M. Mueller, P. G. v. Engen, and K. H. J. Buschow, “New class of materials: Half-metallic ferromagnets,” *Phys. Rev. Lett.* **50**, 2024–2027 (1983).
- ⁵⁰A. Halder, A. Ghosh, and T. S. Dasgupta, “Machine-learning-assisted prediction of magnetic double perovskites,” *Phys. Rev. Mater.* **3**, 084418 (2019).
- ⁵¹S. Sanvito *et al.*, “Accelerated discovery of new magnets in the Heusler alloy family,” *Sci. Adv.* **3**, e1602241 (2017).
- ⁵²C. Tang, C. Zhang, Z. Jiang, K. Ostrikov, and A. Du, “Theoretical discovery of Dirac half metal in experimentally synthesized two dimensional metal semiquinoid frameworks,” *J. Mater. Chem. C* **7**, 5792–5796 (2019).
- ⁵³S. Lu *et al.*, “Coupling a crystal graph multilayer descriptor to active learning for rapid discovery of 2D ferromagnetic semiconductors/half-metals/metals,” *Adv. Mater.* **32**, 2002658 (2020).
- ⁵⁴S. M. Griffin and J. B. Neaton, “Prediction of a new class of half-metallic ferromagnets from first principles,” *Phys. Rev. Mater.* **1**, 044401 (2017).
- ⁵⁵H. C. Kandpal, G. H. Fecher, and C. Felser, “Calculated electronic and magnetic properties of the half-metallic, transition metal based Heusler compounds,” *J. Phys. D: Appl. Phys.* **40**, 1507–1523 (2007).
- ⁵⁶Z. Allahyari and A. R. Oganov, *Multi-objective Optimization as a Tool for Material Design* (Springer International Publishing, Cham, 2020), pp. 2777–2790.
- ⁵⁷M. Núñez-Valdez, Z. Allahyari, T. Fan, and A. R. Oganov, “Efficient technique for computational design of thermoelectric materials,” *Comput. Phys. Commun.* **222**, 152–157 (2018).
- ⁵⁸H. Sims, S. J. Oset, W. H. Butler, J. M. MacLaren, and M. Marsman, “Determining the anisotropic exchange coupling of CrO_2 via first-principles density functional theory calculations,” *Phys. Rev. B* **81**, 224436 (2010).
- ⁵⁹Materials Project, <https://materialsproject.org/>.
- ⁶⁰L. Wang, T. Maxisch, and G. Ceder, “Oxidation energies of transition metal oxides within the GGA + *U* framework,” *Phys. Rev. B* **73**, 195107 (2006).
- ⁶¹A. Jain *et al.*, “Commentary: The materials project: A materials genome approach to accelerating materials innovation,” *APL Mater.* **1**, 011102 (2013).
- ⁶²F. Maldonado, R. Rivera, and A. Stashans, “Structure, electronic and magnetic properties of Ca-doped chromium oxide studied by the DFT method,” *Physica B* **407**, 1262–1267 (2012).
- ⁶³W. H. Cloud, D. S. Schreiber, and K. R. Babcock, “X-ray and magnetic studies of CrO_2 single crystals,” *J. Appl. Phys.* **33**, 1193–1194 (1962).
- ⁶⁴G. P. Singh, S. Ram, J. Eckert, and H.-J. Fecht, “Synthesis and morphological stability in CrO_2 single crystals of a half-metallic ferromagnetic compound,” *J. Phys.: Conf. Ser.* **144**, 012110 (2009).
- ⁶⁵J. Dho, S. Ki, A. F. Gubkin, J. M. S. Park, and E. A. Sherstobitova, “A neutron diffraction study of half-metallic ferromagnet CrO_2 nanorods,” *Solid State Commun.* **150**, 86–90 (2010).
- ⁶⁶W. M. Haynes, *CRC Handbook of Chemistry and Physics* (CRC Press, 2014).
- ⁶⁷A. H. Hill, A. Harrison, C. Dickinson, W. Zhou, and W. Kockelmann, “Crystallographic and magnetic studies of mesoporous eskolaite, Cr_2O_3 ,” *Microporous Mesoporous Mater.* **130**, 280–286 (2010).
- ⁶⁸V. S. Telegus and Yu. B. Kuz’ma, “Ternary phases with the structure of the U_3Si_2 type in the W–Mn–B and Mo–Mn–B systems,” *Dopov. Akad. Nauk Ukr. RSR, Ser. A, No. 10*, 951-3(1968) (in Ukrainian).
- ⁶⁹V. S. Telegus and Y. B. Kuz’ma, “Phase equilibria in the systems vanadium-manganese-boron, molybdenum-manganese-boron, and tungsten-manganese-boron,” *Sov. Powder Metall. Met. Ceram.* **10**, 52–56 (1971).
- ⁷⁰R. Skomski and J. M. D. Coey, “Giant energy product in nanostructured two-phase magnets,” *Phys. Rev. B* **48**, 15812–15816 (1993).
- ⁷¹E. F. Kneller and R. Hawig, “The exchange-spring magnet: A new material principle for permanent magnets,” *IEEE Trans. Magn.* **27**, 3588 (1991).
- ⁷²Since we have a structure with a large unit cell, doing antiferromagnetic calculation would require a supercell of 8 times larger than the unit cell, so practically doing such DFT+*U* calculation for nearly a hundred atoms in a supercell is impossible.

- ⁷³S. Biermann *et al.*, "Observation of Hubbard bands in γ -manganese," *J. Exp. Theor. Phys. Lett.* **80**, 612–615 (2004).
- ⁷⁴I. Di Marco *et al.*, "Correlation effects in the total energy, the bulk modulus, and the lattice constant of a transition metal: Combined local-density approximation and dynamical mean-field theory applied to Ni and Mn," *Phys. Rev. B* **79**, 115111 (2009).
- ⁷⁵D. Korotin *et al.*, "Construction and solution of a Wannier-functions based Hamiltonian in the pseudopotential plane-wave framework for strongly correlated materials," *Eur. Phys. J. B* **65**, 91–98 (2008).
- ⁷⁶V. S. Telegus, "Reaction of Groups VI and VII transition metals with boron," *Khim. Khim. Tekhnol.* **1**, 96–100 (1970).
- ⁷⁷A. Le Bail, H. Duroy, and J. L. Fourquet, "Ab-initio structure determination of LiSbWO_6 by X-ray powder diffraction," *Mater. Res. Bull.* **23**, 447–452 (1988).
- ⁷⁸H. Giefers and M. Nicol, "High pressure X-ray diffraction study of all Fe–Sn intermetallic compounds and one Fe–Sn solid solution," *J. Alloys Compd.* **422**, 132–144 (2006).
- ⁷⁹B. Fayyazi *et al.*, "Experimental and computational analysis of binary Fe–Sn ferromagnetic compounds," *Acta Mater.* **180**, 126–140 (2019).
- ⁸⁰B. C. Sales, B. Saporov, M. A. McGuire, D. J. Singh, and D. S. Parker, "Ferromagnetism of Fe_3Sn and alloys," *Sci. Rep.* **4**, 7024 (2014).
- ⁸¹A. S. Belozherov and V. I. Anisimov, "Coulomb interaction parameters in bcc iron: An LDA + DMFT study," *J. Phys.: Condens. Matter* **26**, 375601 (2014).
- ⁸²A. E. Antipov, I. S. Krivenko, V. I. Anisimov, A. I. Lichtenstein, and A. N. Rubtsov, "Role of rotational symmetry in the magnetism of a multiorbital model," *Phys. Rev. B* **86**, 155107 (2012).
- ⁸³A. Hausoel *et al.*, "Local magnetic moments in iron and nickel at ambient and Earth's core conditions," *Nat. Commun.* **8**, 16062 (2017).
- ⁸⁴J. M. Coey, *Magnetism and Magnetic Materials* (Cambridge University Press, 2010).
- ⁸⁵M. Armbrüster, M. Schmidt, R. Cardoso-Gil, H. Borrmann, and Y. Grin, "Crystal structures of iron distannide, FeSn_2 , and cobalt distannide, CoSn_2 ," *Z. Kristallogr. - New Cryst. Struct.* **222**, 83–84 (2007).
- ⁸⁶C. Echevarria-Bonet *et al.*, "Structural and magnetic properties of hexagonal Fe_3Sn prepared by non-equilibrium techniques," *J. Alloys Compd.* **769**, 843–847 (2018).
- ⁸⁷M. Armbrüster, W. Schnelle, R. Cardoso-Gil, and Y. Grin, "Chemical bonding in compounds of the CuAl_2 family: MnSn_2 , FeSn_2 and CoSn_2 ," *Chem. - Eur. J.* **16**, 10357–10365 (2010).
- ⁸⁸J. A. Flores-Livas, "Crystal structure prediction of magnetic materials," *J. Phys.: Condens. Matter* **32**, 294002 (2020).
- ⁸⁹Y. Zhang, G. J. Miller, and B. P. T. Fokwa, "Computational design of rare-earth-free magnets with the $\text{Ti}_3\text{Co}_5\text{B}_2$ -type structure," *Chem. Mater.* **29**, 2535–2541 (2017).
- ⁹⁰A. Vishina *et al.*, "High-throughput and data-mining approach to predict new rare-earth free permanent magnets," *Phys. Rev. B* **101**, 094407 (2020).
- ⁹¹E. B. Linscott, D. J. Cole, M. C. Payne, and D. D. O'Regan, "Role of spin in the calculation of Hubbard U and Hund's J parameters from first principles," *Phys. Rev. B* **98**, 235157 (2018).